

AN EXPERIMENTAL STUDY ON WATER JET MICRO-BENDING OF A METALLIC SHEET

Jamal-Deen Kukurah, Anthony Akayeti, Philip Yamba
Faculty of Engineering (Mechanical Engineering Department,
Tamale Technical University, Tamale, Ghana

Joseph Sekyi-Ansah
Mechanical Engineering Department,
Takoradi Technical University, Takoradi, Ghana

James Kwasi Quaisie, Abdul-Hamid Mohammed,
Faculty of Engineering (Welding & Fabrication Department,
Tamale Technical University, Tamale, Ghana

Bismark Addai
Materials Engineering Department,
Sunyani Technical University, Sunyani, Ghana

Abstract: Cavitation water jet shock is a manufacturing process, in which a strong shock wave is produced and induces high pressures on the surface of the target material. Mostly, this process is used to improve material properties such as the hardness and fatigue life. The water jet shock bending is a sheet metal micro-forming process using cavitation water jet to accurately bend, shape, precision align, or repair micro-components with bending angles less than 10° . Negative bending angle (away from water jet) can be achieved with the high-incident pressure, in addition to the conventional positive water jet bending mechanism. In this study, various experimental and numerical studies on a cold rolled 304 stainless steel thin sheet were conducted to investigate the different deformation mechanisms, positive and negative. The experiments were conducted with the sheet thickness varying from 0.25 to 1.75 mm and incident pressure of 0.2 to 0.5 MPa. A critical thickness threshold of 0.7-0.88 mm was found that the transition of positive negative bending mechanism occurred. A statistic regression analysis was also developed to determine the bending angle as a function of cavitation water jet process parameters for positive bending cases.

Keywords: Cavitation water jet, strong shock wave, high pressures, sheet metal, micro-bending.

I. INTRODUCTION

In this article, the application of sheet metal bending using the cavitation water jet process is investigated. In order to

address the deformation control technique in water jet micro-bending, where various experiments were conducted on thin aluminum sheet in one-side shock formation. The experiments were conducted using a water jet device. The bending angle evaluated in this study was less than 10° , which is usually the magnitude of deformation error for sheet metal generated in assembly processes. In view of this most studies were conducted by various researchers where Aragon and associates [1] carried out a study on Micro-beam bending of FCC bicrystals: An analysis comparing simulations and observations using defect dynamics. The findings demonstrated that, depending on the properties of the GB, the mechanical response of bicrystals could have both hardness and softening. The micro-bending simulations also showed good agreement with related micro-bending measurements. Furthermore, distinct mechanical reactions are obtained when the GB location in the microbeams is altered. For example, angled GBs positioned midway down the length of the beam have minimal influence, whereas GBs located at the neutral plane exhibit softening relative to single crystals. The mechanical response of bicrystalline samples is analyzed using quantitative resolved shear stress analysis augmented by dislocation density distribution, and simulation results may paint a clear picture of the intricate dislocation-GB interactions. Using in-situ micro-bending tests, Freisinger et al. [2] investigated the mechanical characteristics of near-surface microstructures in tribological contacts. According to their findings, a rail wheel's brown etching layer region exhibits plastic material behavior most prominently. Notable differences in material behavior and fracture propagation are uncovered in specific

areas of the near-surface microstructure of a roller bearing and a self-lubricating laser cladding. The method's ability to get high-resolution insights into material behavior is demonstrated by qualitative analysis and stress-displacement graphs, which further our understanding of the microstructural changes influencing friction, wear, and component failure in tribosystems. A study on the micro-scale fracture toughness measurement techniques of WC-Co cemented carbide material utilizing the micro-bending method and nanoindentation was carried out by Monnet et al. [3]. They used a micro-bending test on pre-notched cemented carbide micro-cantilevers in their study to introduce a linked numerical-experimental approach to evaluate the stress intensity factor at the microscale. Micro-electrical-discharge milling is utilized to construct the specimens, and focused ion beam processing is employed to create the initial crack in order to guarantee a repeatable crack form. Beam theories are verified by defining geometries. A study on the correlation between sample geometry and grain size in electrodeposited polycrystalline gold micro-bending was carried out by Suzuki et al [4]. In this work, correlations between the average grain size and the effect of sample geometry on the bending characteristics are assessed while micro-cantilevers made of electrodeposited gold are created using a focus ion beam system. To determine how each sample geometry effect and average grain size contribute to the micro-mechanical strength, the average grain size of all as-fabricated micro-cantilevers is determined. Wu and associates [5] The mechanism of cold-rolled tungsten's increased ductility at room temperature under micro bending tests. According to their work, a CR tungsten micro-cantilever fractures in the L-T fracture system in a semi-brittle way, as revealed by three-dimensional electron backscatter diffraction. The blunted, ductile region has considerable dislocation mobility in the direction away from the cracking point, and low-angle

grain boundaries are highly linked with its emission pathway. In the meantime, stress cracking and brittle intergranular fracture are caused by strain and dislocations that are stopped at high-angle grain boundaries. The crack bridging effect is caused by these brittle and ductile failure modes, which eventually result in controlled fracture propagation. This approach might yield useful insights for further studies on the increase of ultra-fine grain W ductility. Therefore, the technique presented in this study can be used to align the sheet to the desired dimensions. The effects of incident pressure, scanning scheme, and sheet thickness were examined and the bending Mechanisms (Positive and Negative) were numerically analyzed.

II. MATERIALS AND METHODS

2.1 Materials

In this experiment, a cold rolled 304 stainless steel sheet were selected as the specimen due to their resistance to corrosion and excellent mechanical properties. Thus, 304 stainless steel sheet with the thickness of 0.7, 0.88, 1.07, and 1.75 mm was used. A schematic of the specimen constraint and how the bending angle is measured after the experiment is shown in Figure 1. The profile of the bending angle was captured by a JGX-type 1 microscope and the edge lines of the image were detected by an image processing software. The bending angle could then be obtained by calculating the difference in the slopes of the two edge lines. The measurement had an accuracy of 1' per measurement. A positive bending angle was defined as bending towards the laser beam, while a negative bending angle is defined as bending away from the laser beam, as depicted in Figure 16. It should be noted that the bending angle evaluated in this study was less than 10° , which is usually the deformation problem of sheet metal generated in the assembly process [6].

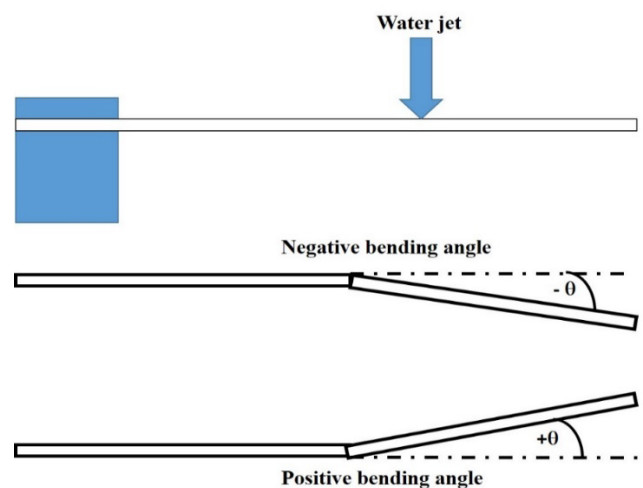


Fig. 1 Bending angle measurement.

Table 1 shows the mechanical properties of the 304 stainless steel sheet.

Table 1 The mechanical properties of 304 stainless steel foils.

Thickness R (μm)	Angle to rolling direction (°)	Young modulus E (GPa)	Yield point σ_o (MPa)	Tensile strength σ_{ult} (MPa)	K (MPa)	n
100	0	154.5	277.1	580.4	1350.6	0.4517
	45	197	252.4	539.1	1269.8	0.4345
	90	166	287.2	621.7	1400.3	0.4104

2.2 Experimental setup

The setup for water jet cavitation shock bending experiments conducted for this investigation is shown in Figure 2. Tap water was reserved for at least 20 hours before the test in a large tank of size 1.5 m×2 m×2.5 m, with a temperature of 24 ± 3 °C. The experiments are carried out using a water tank (transparent) having a height of 800 mm and a square horizontal cross-sectional area of 400 mm × 400 mm. Due to the visualization flow purpose, the tank is made of acrylic resin. The nozzle, which was designed with reference to the angular nozzle for generating the periodic behavior of the water jets cavitation [7] for this experiment, is as shown in Fig. 3. The ratio of the optimum size is $d:L = 1:8$ [8], where the throat diameter d of the nozzle is 1.5 mm, the throat length L is 12 mm. The nozzle was situated 160 mm deep from the surface of the water and the flow through the nozzle was driven using the plunger pump to generate

the submerged cavitation jets in the high-pressure test cell. The diameter and the depth of the micro-die cavity are about 1.2 mm and 3 mm, respectively. The upstream and downstream pressure of the nozzle was measured by the pressure transducer. In the present paper, the pressures are absolute pressures. Although the maximum operating pressure of the plunger pump is 30 MPa, most of the experiments are carried out at 4-10 MPa. The blank holder force was 26N, which can have inhibited the radial flow of material. The standoff distance S is defined as the distance between the nozzle outlet and the surface of the specimen under test. Before the incident pressure impact, the specimens were cleaned with acetone. The experimental conditions are given in Table 2. The specimen thickness was varied from 0.7 to 1.75 mm, incident pressure from 4 to 10 MPa, duration time of 2 minutes and the standoff distance of 120 m per test were used.

Table 2 experimental conditions

Parameters	value
Pressure (P)	4MPa 6MPa 8MPa 10MPa
Standoff distance (S)	120mm
Time (t)	2min
Die diameter (\varnothing)	1.2mm
Depth (h)	3mm
Nozzle angle (θ)	30°
Blank holder force (F)	26N

(a)

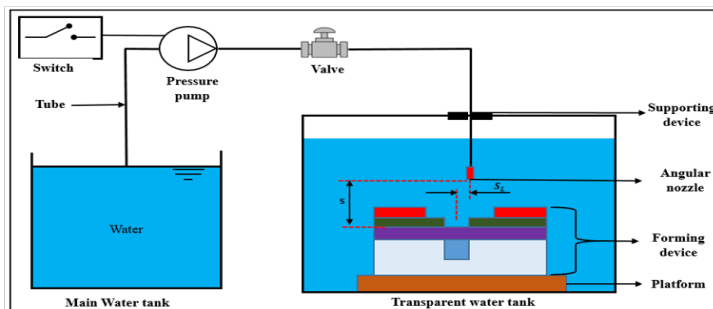


Fig. 2 Experimental system of water jet shock for sheet metal bending.

(b)

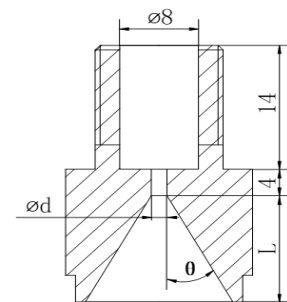


Fig. 3 Nozzle geometry diagram.

III. RESULTS AND DISCUSSION

3.1 Effect of incident pressure on the Bending Mechanism

Figure 4 displays the bending angles with various laser pulse energy for various specimen thicknesses. In the 0.7 mm thick specimen, positive bending was clearly visible, however the 1.07 and 1.75 mm thick specimens seemed to exhibit more negative bending. When the incidence pressure was low (4–5 MPa), no visible bending was seen for the specimen with a thickness of 0.88 mm; nevertheless, when the incident pressure increased to 8–10 MPa, a positive bending angle of roughly 27° was measured. Because the

incident pressure for thinner specimens (<0.88 mm) is proportional to deformation, a higher incident pressure is associated with a bigger positive bending angle. For example, for specimens with a thickness of 0.7 mm, the sheet bending angle increased from 65° to 133° when the incident pressure increased from 4 to 10 MPa. There is no discernible impact of incident pressure on the bending angle for the negative bending angle. The same is seen in Figure 4. For 1.07- and 1.75-mm thick specimens, it seemed that the negative bending angle saturated at about -15° and -30°, respectively [9].

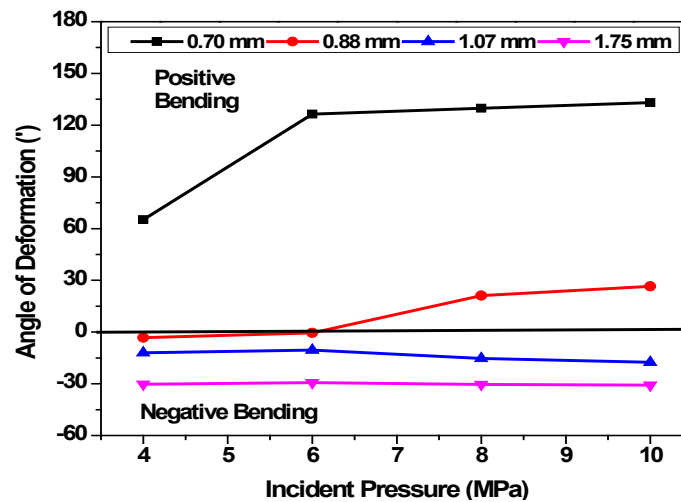


Fig. 4. Relationship between energy and bending angle.

3.2 Effect of Sheet Thickness on the Bending Mechanism

The impact of specimen thickness on the bending process is investigated in Figure 5. The bending angle changes from positive to negative as the specimen thickness grows, suggesting that the specimen thickness is the primary factor influencing the positive-negative bending transition. A positive bending angle was attained for incoming pressures

ranging from 0.2 to 0.5 MPa using thin specimens (0.7 mm). For all examined laser pulse energy, a negative bending angle was obtained when the specimen thickness reached 1.07 mm or above. As the thickness of the specimen increases beyond 0.88 mm, the mechanism appears to shift from a positive to a negative bending angle, marking the transition position [9].

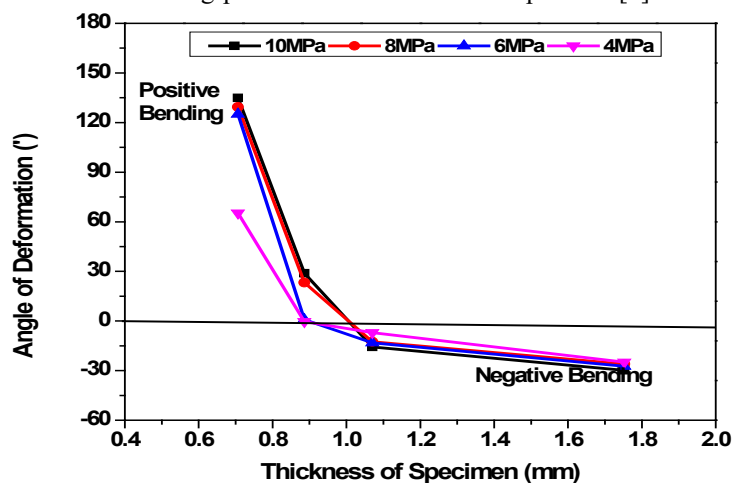


Fig. 5. Relationship between sheet thickness and bending angle.



IV. CONCLUSION

When determining the deformation of the water jet micro-bending, the specimen thickness and incidence pressure turned out to be the most important elements. The test findings demonstrated that, given identical incidence pressure parameters, the specimens' thickness plays a major role in identifying the sheet's deformation mechanism. The 0.25 mm thick sheet's deformation mechanism will be positive under all incident pressure conditions, whereas the 1.75 mm thick sheet's deformation mechanism will be negative under all incident pressure conditions, as demonstrated by a comparison of the thickest specimen (1.75 mm) and the thinnest specimen (0.25 mm). It was discovered that incident pressure only mattered for the water jet parameters when the sheet metal's thickness was less than the transition thickness, which is roughly 0.88 mm. Then, in the positive deformation mechanism settings, the incident pressure had increasingly notable positive impacts on the sheet's deformation as the specimen thickness decreased. When the incident pressure increases, the bending angle for the negative bending mechanism changes very little. Additionally, it seems that the negative bending angle saturates at a specific value, at -15° and -30° for specimens that are 1.07 and 1.75 mm thick, respectively. As was previously indicated, the switch from positive to negative bending mechanism was observed to occur at a crucial thickness barrier of 0.7–0.88 mm. The deformation mechanism is positive when the thickness is less than the threshold and negative when the thickness is more than the threshold.

V. REFERENCE

- [1]. Aragon, N. K., Na, Y.-e., Nguyen, P. C., Jang, D., & Ryu, I. (2023). Micro-beam bending of FCC bicrystals: A comparison between defect dynamics simulations and experiments. *Materialia*, 32, 101941. doi: <https://doi.org/10.1016/j.mtla.2023.101941>
- [2]. Dewil, R., Vansteenwegen, P., & Cattrysse, D. (2015). Sheet metal laser cutting tool path generation: dealing with overlooked problem aspects. *Key Engineering Materials*, 639, 517-524.
- [3]. Freisinger, M., Rodríguez Ripoll, M., & Hahn, R. (2024). Unveiling the mechanical properties of near-surface microstructures in tribological contacts via in-situ micro-bending tests. *Tribology International*, 191, 109190. doi: <https://doi.org/10.1016/j.triboint.2023.109190>
- [4]. Monnet, J., Gaillard, Y., Richard, F., Personeni, M., & Thibaud, S. (2024). Fracture toughness determination methods of WC-Co cemented carbide material at micro-scale from micro-bending method using nanoindentation. *Journal of Materials Research and Technology*, 28, 1370-1381. doi: <https://doi.org/10.1016/j.jmrt.2023.12.071>
- [5]. Mu, Y., Feng, R., Gong, Q., Liu, Y., Jiang, X., & Hu, Y. (2021). A flexible two-sensor system for temperature and bending angle monitoring. *Materials*, 14(11), 2962.
- [6]. Quaisie, J. K., Yun, W., Zhenying, X., Chao, Y., Li, F., Baidoo, P., . . . Asamoah, E. (2020). Experimental Study on Water-Jet Shock Microforming Process Using Different Incident Pressures. *Advances in Materials Science and Engineering*, 2020, 1-9.
- [7]. Suzuki, K., Jiang, Y., Hori, R., Hashigata, K., Kurioka, T., Chen, C.-Y., . . . Sone, M. (2023). Correlation of sample geometry and grain size in micro-bending of electrodeposited polycrystalline gold. *Materials Today Communications*, 35, 106072. doi: <https://doi.org/10.1016/j.mtcomm.2023.106072>
- [8]. Wu, X., Jimba, Y., Kondo, S., Yu, H., Ogino, Y., Hasegawa, A., & Kasada, R. (2024). Mechanism of enhanced room temperature ductility of cold-rolled tungsten under micro-bending test. *Materialia*, 33, 101971. doi: <https://doi.org/10.1016/j.mtla.2023.101971>
- [9]. Zhao, G., Liang, N., Zhang, Y., Cao, L., & Wu, D. (2021). Dynamic behaviors of blade cavitation in a water jet pump with inlet guide vanes: Effects of inflow non-uniformity and unsteadiness. *Applied Ocean Research*, 117, 102889.